

Automated fast label-free quantification of cardiomyocyte dynamics with raw holograms for cardiotoxicity screening

INKYU MOON, 1,* DEZAT AHMADZADEH, 1 YOUHYUN KIM, 1 BENJAMIN RAPPAZ, 2 AND GERARDO TURCATTI 2

Abstract: Traditional cell analysis approaches based on quantitative phase imaging (QPI) necessitate a reconstruction stage, which utilizes digital holography. However, phase retrieval processing can be complicated and time-consuming since it needs numerical reconstruction and then phase unwrapping. For analysis of cardiomyocyte (CM) dynamics, it was reported that by estimating the spatial variance of the optical path difference from QPI, the spatial displacement of CMs can be quantified, thereby enabling monitoring of the excitation-contraction activity of CMs. Also, it was reported that the Farnebäck optical flow method could be combined with the holographic imaging information from QPI to characterize the contractile motion of single CMs, enabling monitoring of the mechanical beating activity of CMs for cardiotoxicity screening. However, no studies have analyzed the contractile dynamics of CMs based on raw holograms. In this paper, we present a fast, label-free, and high throughput method for contractile dynamic analysis of human-induced pluripotent stem cell-derived CMs using raw holograms or the filtered holograms, which are obtained by filtering only The proposed approach obviates the need for timeconsuming numerical reconstruction and phase unwrapping for CM's dynamic analysis while still having performance comparable to that of the previous methods. Accordingly, we developed a computational algorithm to characterize the CM's functional behaviors from contractile motion waveform obtained from raw or filtered holograms, which allows the calculation of various temporal metrics related to beating activity from contraction-relaxation motion-speed profile. To the best of our knowledge, this approach is the first to analyze drug-treated CM's dynamics from raw or filtered holograms without the need for numerical phase image reconstruction. For one hologram, the reconstruction process itself in the existing methods takes at least three times longer than the process of tracking the contraction-relaxation motion-speed profile using optical flow in the proposed method. Furthermore, our proposed methodology was validated in the toxicity screening of two drugs (E-4031 and isoprenaline) with various concentrations. The findings provide information on CM contractile motion and kinetics for cardiotoxicity screening.

© 2025 Optica Publishing Group under the terms of the Optica Open Access Publishing Agreement

1. Introduction

Digital holographic microscopy (DHM) is a well-known imaging method for applications in the field of cell biology and recovering complicated field information from label-free microscopic samples [1,2]. DHM is a promising tool to noninvasively analyze the dynamics of transparent or semitransparent cells, such as temporal fluctuations and spatiotemporal dynamics of live red blood cells (RBCs) [3–5]. Quantitative phase digital holographic microscopy (QP-DHM) is a label-free method of acquiring high-speed quantitative phase images of cell architecture and dynamics. DHM can be used for dynamic cell identification and analysis with single exposure

#542362 Journal © 2025 https://doi.org/10.1364/BOE.542362

¹ Department of Robotics & Mechatronics Engineering, Daegu Gyeongbuk Institute of Science & Technology (DGIST), Dae-gu 42988, Republic of Korea

²Biomolecular Screening Facility, Ecole Polytechnique Fedérale de Lausanne (EPFL), Lausanne 1015, Switzerland

^{*}inkyu.moon@dgist.ac.kr

[6,7]. Human cardiomyocytes (CM) formed from human-induced pluripotent stem cell (hiPSC) dynamics, which are transparent or semitransparent tiny objects, can be accurately quantified using DHM [1–13]. CM physiological characteristics (dry mass redistribution) are altered by drugs that produce cardiac arrhythmias, such as changes in contraction-relaxation motion-speed, beating frequency, contraction period, relaxation period, and motion patterns [14–16]. As a result, DHM is particularly useful for investigating CM dynamics in a label-free way, highly relevant information about cell dynamics of dry mass redistribution can be collected [17–19].

DHM is capable of single-shot holographic recording, allowing for real-time phase imaging. Since DHM can perform numerical focusing by numerical wavefront propagation, there is no need to record focused images of the specimen on a digital detector [20]. DHM allows fast scanning of surfaces without the vertical mechanical movements required to focus on an object in other types of microscopes. DHM is capable of automatic digital focus. As a result, the depth of field of high NA microscope objectives is expanded numerically. The numerical propagation associated with digital optics and automatic fitting procedures allows vibration-insensitive full-field phase imaging and full a priori compensation for image distortions and/or phase aberrations [20]. Additionally, DHM may be optically complex (interferometry), but as an economical option in the field of microscopy, fewer lenses and objectives are required for the microscope to function as laser diodes and image sensors take their place, making the components of a digital holographic microscope relatively inexpensive.

For the CM dynamic analysis, current off-axis holographic processing necessitates the production of optical path difference (OPD) maps. In this procedure, digital spatial filtering in Fourier domain is required to clearly obtain only the real image from a hologram of CMs, resulting in a filtered hologram [19,21]. Reconstruction of DHM holograms, thereby retrieving information of the cells from the hologram, requires the numerical calculation of Fresnel propagation and the phase compensation [22–25]. Then, the phase argument is subjected to the two-dimension (2D) phase unwrapping technique to resolve the 2π phase discontinuity [26]. However, reconstructing object images from complex diffraction patterns for cell dynamic analysis requires extensive computations. To overcome this issue, high-throughput pre-clinical cardiac safety assessment methods, which yield CM characterization without hologram reconstruction, are needed. While there have been attempts for a fast transformation, they still take non-negligible time for CM characterization, including patch clamping [27,28], calcium imaging and/or calcium transients [29–31], and image processing-based contraction-relaxation studies [32,33]. All the abovementioned methods require expensive equipment or specific expertise, which demonstrates the shortcomings in simplified methods for CM motion characterization.

We want to save the processing time of the hologram reconstruction to the quantitative phase profile of the cell. In this work, we aim to propose a novel automated approach to CM dynamic analysis that skips the pre-processing of creating OPD maps and directly uses the holographic images. Optical flow-based motion tracking provides low-cost, high-throughput solutions for measuring CM contractile activity without making physical contact with the sample, preserving the sample's integrity [34,35]. The Farnebäck optical flow method, which is the dense optical flow method, tracks objects by measuring the displacement of each pixel in an image, ideal for CM contractile kinetic analysis [36]. We previously reported low-cost, high-throughput single CM motion characterization using QP-DHM imaging informatics and the Farnebäck optical flow method [37]. This method enables CM motion characterization at the single-cell level, as well as the quantification of several parameters.

We report on an alternative approach, which allows dynamic information of CMs to be extracted from the hologram, skipping the pre-processing stage of calculating the OPD maps while achieving comparable performance. The cardiomyocyte's hologram images were obtained using DHM. Then, the Farnebäck optical flow method was applied to monitor the dynamic and rhythmic beating patterns, and a biomechanical contractile motion waveform was generated. After

treatment with E-4031 and Isoprenaline, the system was able to detect cardiac functional behavior sensitively and quantitatively. Following this, a computational algorithm was implemented to quantify the contractile motion of CM from the motion waveform signal, and several parameters related to the periodicity of the CM beating activity profile were calculated. The quantification parameters include contraction motion-speed, relaxation motion-speed, contraction period, relaxation period, and resting period, beating period, and beating rates. In comparison to the control, the E-4031 compound slows down the contraction-relaxation motion, whereas Isoprenaline speeds up the contraction-relaxation motion. Finally, the suggested method's sensitivity in efficiently detecting the periodicity of the beating profile makes it well-suited to the early preclinical safety assessment of cardiotoxic substances.

2. Material and methods

2.1. Cardiomyocyte cell preparations

Human-induced pluripotent stem cell-derived CM obtained from Cellular Dynamics Int. (Madison, WI) were cultured and grown according to the manufacturer's instructions for 14 days before recording a QPI. Measurements were acquired in a Chamlide WP incubator system with a 96-well plate (LCI, South Korea) set at 37° and 5% CO₂ with high humidity. Images were recorded with the commercially available DHM T-1001 from LynceeTec SA (Lausanne, Switzerland) equipped with a motorized stage (Märzhäuser Wetzlar GmbH & Co. KG, Wetzlar, Germany, ref. S429). Images were obtained using a Leica $20\times/0.4$ NA Objective finder (Leica Microsystems GmbH, Wetzlar, Germany, ref. 11566049). The QPIs of CM were acquired at a 50 Hz sampling frequency for 30 seconds. For the control condition, a sequence of QPIs was recorded before treatment. Following this, the drugs were added at different concentrations in individual wells. Experiments were conducted in triplicate (three separate wells with one $300\times300~\mu m$ field acquired per well containing about 50 cells). For the E-4031 drug-treated research, time-lapse photos were acquired for 60 seconds at a sampling frequency of 10~Hz, and for the isoprenaline treatment, 50~Hz (30 seconds). The faster pounding generated by isoprenaline necessitated an increase in the sample rate in the latter scenario.

2.2. Digital holographic imaging

In the off-axis DHM, as shown in Fig. 1(a), a raw hologram created by the interference of the object wave (O) and the reference wave (R) incident at a slight angle θ is recorded on the CCD camera, as shown in Fig. 1(b). The Fourier transformation of the raw hologram is used to get three separated major bandwidths (or spectra) corresponding to the real image, the twin or virtual image, and the zero-order noise in the Fourier domain, as illustrated in Fig. 1(c). Among these spectra, a spatial filter can be used to pass only the spectrum of the real image, thereby obtaining a filtered hologram, i.e., Fig. 1(e) [21]. Finally, the phase image of CMs from the filtered hologram is calculated using numerical reconstruction algorithms, as shown in Fig. 1(f) [22,23,38].

2.3. Analysis of contractile dynamics of CMs based on OPD

Upon excitation-contraction activity of CMs, cell movement of CMs can be monitored by quantitatively estimating the spatial variance of OPD [39,40], which changes due to cell shape modification and dry mass redistribution. Since the OPD is more relevant in the analysis of biological sample, the phase value $\varphi=(2\pi/\lambda)\times OPD$ and OPD are used interchangeably, where λ is the wavelength of the illumination light. The OPD value can be represented by the difference in integral refractive index between intracellular content and the culture medium and the thickness of the cultured sample. The OPD beating signal is related to the cell thickness, which implies movement of the cell in the direction of the optical axis, i.e., in the z direction in Fig. 1(a). The

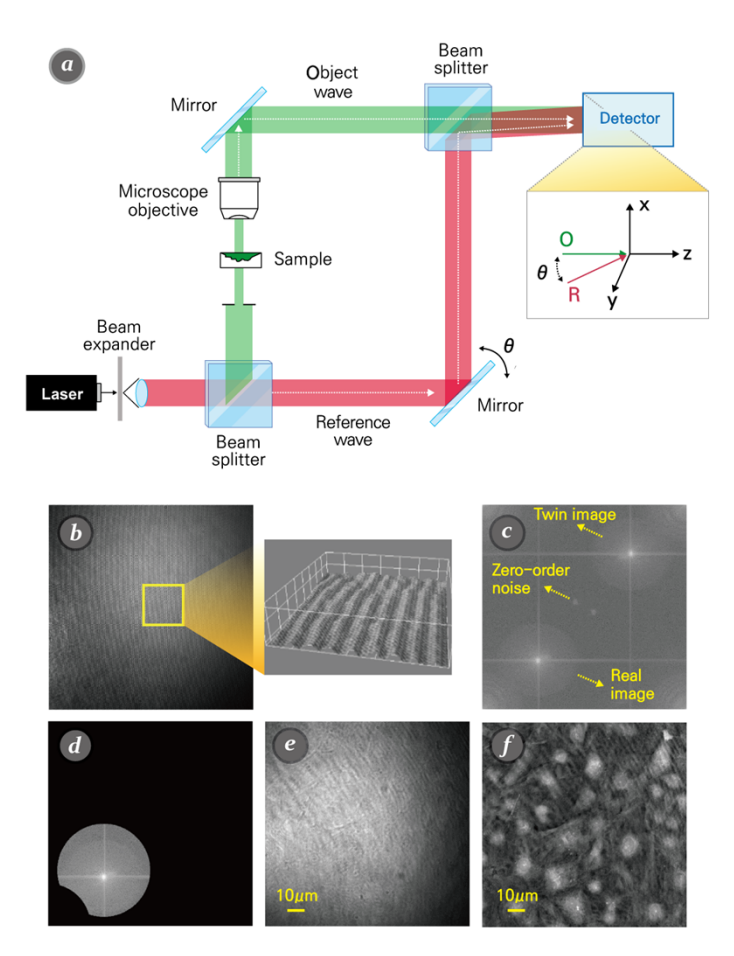


Fig. 1. (a) A schematic of off-axis digital holographic microscopy (DHM), which is employed to get holograms of cardiomyocytes (CMs). (b) A recorded raw hologram of a control cardiomyocyte sample. The inset in the recorded hologram shows a three-dimensional (3D) portion of the hologram. (c) The Fourier spectrum of the hologram, (d) the filtered Fourier spectrum (corresponding the real image), (e) the filtered hologram (corresponding the real image), (f) the reconstructed phase image (RPI) after numerical reconstruction and phase unwrapping. The phase image provides high-contrast data for quantitative analysis.

physical contraction-relaxation activity of CMs' beating can be obtained as [39,40]:

$$OPD_{var}^{n} = var[OPD^{n} - OPD^{n+1}], (1)$$

where OPD^n is obtained from the *n*-th phase image of video of phase images and OPD^{n+1} is obtained from the (n+1)-th phase image, and $var[\cdot]$ is the spatial variance operation.

This equation quantifies the amount of spatial displacement and temporal variance signal between successive frames of the video and represents the contractile behavior. The normal beating activity of CMs can be represented by the two-peak signal associated with contraction and relaxation processes. Since the OPD-variance profiles may have temporal and spatial noise, which may arise from shot noise, speckle, and contributions from out-of-focus structures in the stack, as pre-processing, a 3D median filter with the size of $2 \times 2 \times 2$ can be applied to the reconstructed phase images (RPIs) to remove the noise. Furthermore, the dynamic contraction-relaxation beating activity can be estimated by generating a series of motion vectors, which reveals the

beating activity of CMs in its lateral direction (*x-y* direction), by applying the Farnebäck optical flow method to the phase image reconstructed from the hologram, e.g., Fig. 1(f).

2.4. Analysis of contractile dynamics of CMs based on optical flow

Optical flow may be defined as the 2D displacement field that describes the apparent motion of 3D motives projected in the imaging plane [41]. It is normally determined by evaluating changes in the position of brightness patterns between two successive images. In the sparse optical flow [42], the flow vectors provide only some salient image features such as corners or edges. Because it uses a narrow window, if a large movement than the window occurs, it cannot calculate the movement, and since only feature points are used, accuracy may be low. In contrast, the dense optical flow calculates flow vectors for all image pixels, then the calculation process is complicated and takes a long time [36]. Nevertheless, the Farnebäck optical flow method was utilized to analyze the pharmacological effects of substances on a CM contractile motion waveform. Ahamadzadeh et al. proposed a novel low-cost, fully automated platform to quantitatively analyze the dynamics of hiPS-CMs at the single-cell level by combining Farnebäck optical flow method and holographic imaging informatics, which eliminates the need for expensive equipment to monitor the mechanical beating activity of CMs [37].

For displacement estimation, the Farnebäck approach employs polynomial expansion at multi-resolution levels. In the first stage, the method uses Gaussian pyramids to build multi-resolution levels from the original image, with each level having a lower resolution than the previous level. The tracking procedure begins at the lowest resolution and progresses to the highest. The tracking points detected at each level are considered the starting point for the next level. A substantial displacement can be identified utilizing multi-resolution-level tracking. An example of the pixel motion detection using the optical flow method and multi-resolution image leveling is shown in Fig. 2. The tracking is refined in each resolution level, initializing from the lowest to the highest resolution level. The tracking point detected at each level is the base point for the next level, and the large displacement can be detected. Figure 2(b) shows the optical flow method for estimating pixel displacement in two consecutive image frames, where I(x,y,t) represents the pixel position in the reference frame at time t and I(x + dx, y + dy, t + dt) denotes the pixel displacement in the subsequent frame (the current frame).

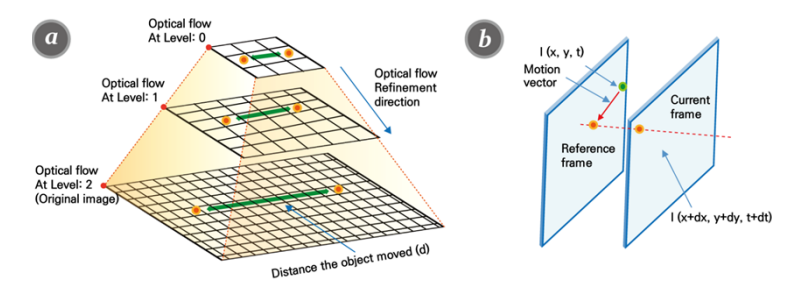


Fig. 2. Pixel motion detection using the optical flow method and multi-resolution image leveling. (a) Three-level multi-resolution leveling of the image. Where tracking starts is the lowest level and where it ends is the highest level. (b) An illustration of the optical flow approach for estimating pixel displacement. Yellow pixels represent the pixel location at time t + dt and black pixels represent the pixel position at time t.

As a result, the following equation is used to determine the displacement of two local patches in consecutive image frames [36]:

$$I(\mathbf{x}) \approx \mathbf{x}^T \mathbf{A} \mathbf{x} + \mathbf{b}^T \mathbf{x} + c, \tag{2}$$

where $\bf A$ stands for symmetric matrix, $\bf b$ is a vector, and c is an unknown scalar. The following equation is used to approximate the first neighborhood:

$$I_1(\mathbf{x}) = \mathbf{x}^T \mathbf{A}_1 \mathbf{x} + \mathbf{b}_1^T \mathbf{x} + c.$$
 (3)

Vector **d** is used to consider the neighborhood's displacement. The following formula is used to compute the new neighborhood resulting from displacement **d**:

$$I_{2}(\mathbf{x}) = I_{1}(\mathbf{x} - \mathbf{d}) = (\mathbf{x} - \mathbf{d})^{T} \mathbf{A}_{1}(\mathbf{x} - \mathbf{d}) + \mathbf{b}_{1}^{T}(\mathbf{x} - \mathbf{d}) + c_{1}$$

$$= \mathbf{x}^{T} \mathbf{A}_{1} \mathbf{x} + (\mathbf{b}_{1} - 2\mathbf{A}_{1} \mathbf{d})^{T} \mathbf{x} + \mathbf{d}^{T} \mathbf{A}_{1} \mathbf{d} - \mathbf{b}_{1}^{T} \mathbf{d} + c_{1}$$

$$= \mathbf{x}^{T} \mathbf{A}_{2} \mathbf{x} + \mathbf{b}_{2}^{T} \mathbf{x} + c_{2}.$$
(4)

Then, $I_2(\mathbf{x})$ and $I_1(\mathbf{x}-\mathbf{d})$ yields $\mathbf{A}_2 = \mathbf{A}_1$, $\mathbf{b}_2 = \mathbf{b}_1 - 2\mathbf{A}_1\mathbf{d}$, and $c_2 = \mathbf{d}^T\mathbf{A}_1\mathbf{d} - \mathbf{b}_1^T\mathbf{d} + c_1$ by using different coefficients from two polynomials. The following equation is used to calculate the distance \mathbf{d} that is used to approximate the optical flow:

$$\mathbf{d} = -\frac{1}{2}\mathbf{A}_1^{-1}(\mathbf{b}_2 - \mathbf{b}_1). \tag{5}$$

By applying the Farnebäck optical flow method, which is the dense optical flow, to raw holograms acquired using DHM, we can monitor the temporal parameters related to the contraction-relaxation motion dynamics of the CM by tracking the contractile motion over the whole-slide images of the CM. The displacement by which CMs have moved can be represented as $\mathbf{d} = d_x \hat{\mathbf{x}} + d_y \hat{\mathbf{y}}$, where d_x and d_y are displacements in x and y directions, which are estimated using the Farnebäck optical flow method from consecutive frames of video, and $\hat{\mathbf{x}}$ and $\hat{\mathbf{y}}$ denote unit vectors in the x and y directions. Then, the magnitude of the displacement can be calculated from the CM motion (CCM) between two consecutive frames of video as follows:

$$D_{CCM} = |\mathbf{d}| = \sqrt{(d_x)^2 + (d_y)^2}.$$
 (6)

The velocity can be represented by $\mathbf{v} = \mathbf{d}/dt = (d_x \,\hat{\mathbf{x}} + d_y \,\hat{\mathbf{y}})/dt$, where dt is considered as the time between two consecutive frames of video. During spontaneous contraction-relaxation beating activity, the motion waveform was derived from CM's motion-speed calculation using the following equation:

$$Speed_{CCM} = |\mathbf{v}| = \sqrt{(d_x)^2 + (d_y)^2}/dt$$
. (7)

2.5. Proposed rapid contractile dynamics analysis of CMs

For OPD-based beating signal, the movement information of the CM along the optical axis, and indirectly the lateral movement information, can be obtained by simply subtracting the OPD on successive frames of video in the time-lapse recording [39,40]. However, for raw and filtered holograms, the lateral movement of the CM in the *x* and *y* directions in Fig. 1(a), can be estimated using the Farnebäck optical flow method. Figure 3 shows the overall workflow for dynamic contraction-relaxation tracking from video of filtered holograms, which is shown in Fig. 1(e) as an example. Dynamic contraction-relaxation tracking for raw holograms follows the same workflow as shown in Fig. 3. After filtering out unwanted spectra from the raw hologram of the drug-treated CM, as shown in Fig. 1(d), the pixel displacement of the filtered hologram of the CM can be estimated using the Farnebäck optical flow method. Steps of the optical flow method for cardiac motion tracking are shown in Fig. 3(b). As an example of a representation of the optical flow method for pixel displacement estimation, a close-up filtered hologram and a close-up raw hologram with superimposed motion vectors is shown in Fig. 3(c) along with CM contractile motion and corresponding heat map. After one beating cycle (contraction-relaxation),

the cell enters the resting state in which the motion vectors show no direction. The overall beating activity profile obtained using motion-speed calculation is shown in Fig. 3(d). The recorded holograms with multiple CMs had a resolution of 1024×1024 pixels.

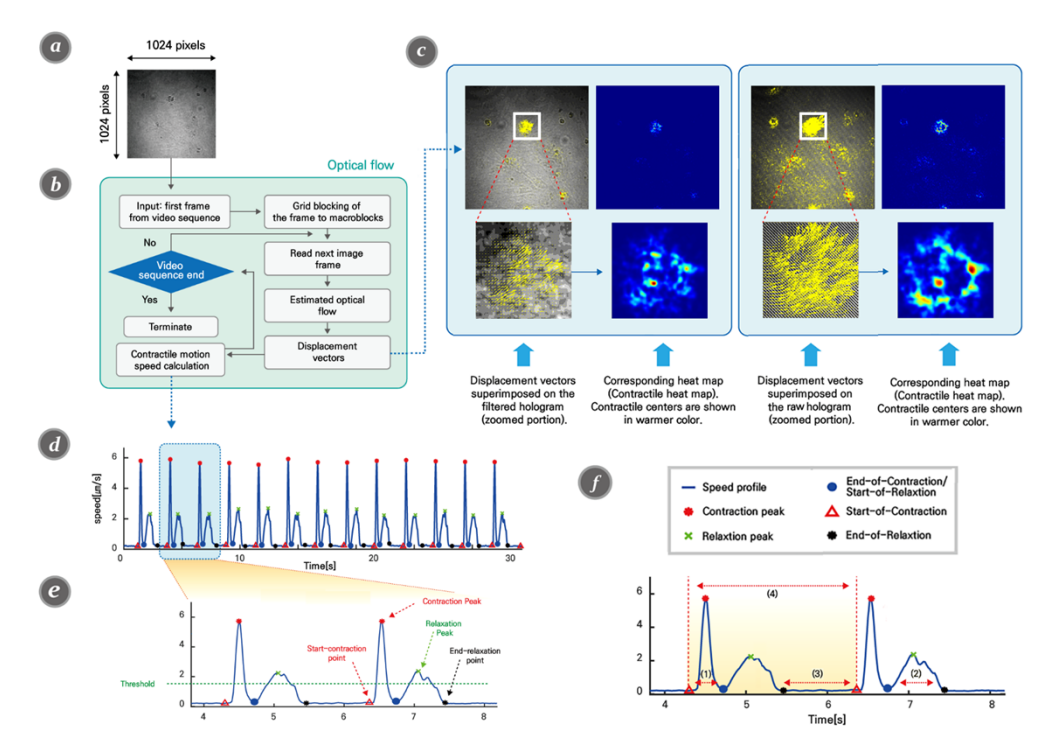


Fig. 3. Schematic of the workflow for motion-speed tracking of CMs and motion waveform extraction using Farnebäck optical flow method. (a) Filtered hologram of drug-treated CMs. (b) The steps of optical flow method for CM motion estimation. (c) A representation of the optical flow method for pixel displacement estimation. Close-up filtered hologram and close-up raw hologram with superimposed motion vectors with CM contractile motion and corresponding heat map. (d) An example of CM's beating activity profile motion waveform generated using the contractile motion-speed calculation. (e) Strategies for multiple point identification beating activity profile. (f) Details of the multiple parameters calculated from the beating activity.

During the beating activity of CMs, an array of motion vectors, which show the CM's motion direction, is generated by repeating the optical flow procedure as shown in Fig. 3(b), resulting in the kinetics waveform. We extracted several parameters related to the contractile motion profile. The estimated CM motion-speed profiles, CM two-peak beating profiles, allow the extraction of several parameters that are highly relevant for characterizing the effects of drugs on CMs utilizing the peak finding approach [40]. The features of CM's beating activity are calculated utilizing two primary peaks from contraction-relaxation and three auxiliary points: start-of-contraction, end-of-contraction, and end-of-relaxation in our suggested technique. Details on accurate peak detection, along with the auxiliary points, were described in our previous study [43].

To define the dynamic beating profile activity of CMs, we first used the Otsu thresholding approach to discover two primary peaks of contraction and relaxation by finding the local maxima of the signal and sorting the peaks by height (see Fig. 3(d) and Fig. 3(e)). Contraction is represented by the first peaks, which have a bigger amplitude value in most circumstances which stands for maximum contraction motion-speed, and relaxation is represented by the

second peaks, which have a lower amplitude value usually used as maximum relaxation motion-speed. The contraction and relaxation peaks are then used to define three auxiliary points: 1) Start-of-Contraction, 2) End-of-Contraction, and 3) End-of-Relaxation. The auxiliary Start-of-Contraction and End-of-Relaxation points are found by searching the span around the peaks of contraction and relaxation. Details of the various parameters calculated from the beating activity are shown in Fig. 3(f). The extracted beating activity-related parameters for every single cell are explained as follows. 1) Contraction period (see #1 in Fig. 3(f)): The average time between the start-of-contraction and end-of-contraction points; 2) Relaxation period (see #2 in Fig. 3(f)): The average time between start-of-relaxation and the end-of-relaxation; 3) Resting period (see #3 in Fig. 3(f)): The average time between end-of-relaxation and the next start-of-contraction; 4) Beating period (see #4 in Fig. 3(f)): The time between two adjacent start-of-contractions.

3. Results

We examine the cardiotoxicity assays of the various substances employed in this work, examining the various characteristics that can discriminate between putative drug modes of action. Due to the direct impacts of the drugs on specific ion channels [15,44], we first investigate a compound's influence on variations of beating rates (or beating frequency) in waveforms, comparing control and drug-treated circumstances. In the contractile motion patterns of numerous hiPSCs' whole-slide raw hologram, changes in beating rates (or beating frequency) appear depending on the mode of action of the compound compared to control conditions. The drug's influence on the motion waveform is revealed in the form of a change in the beating rate. We simulated numerically using Matlab R2023b on the computer with Intel Core i5-13400F @ 2.50 GHz and 32 GB RAM.

3.1. Comparison of contractile dynamics of CMs

Figures 4(a) and 4(b) show the contractile beating profiles of CMs obtained by existing methods, i.e., calculating the variance of the OPD difference between successive RPIs (OPD $_{var}$ -RPI), and applying optical flow to them (Speed-OptF-RPI), respectively, for Isoprenaline control, as an example. Similar to the case of OPD $_{var}$ -RPI, we additionally calculated the variance of the intensity difference between successive raw and filtered holograms. The contractile beating profiles of CMs obtained by calculating the variance of the intensity difference between successive raw and filtered holograms (Int $_{var}$ -Raw-Holo and Int $_{var}$ -Filtered-Holo) is shown in Fig. 4(c) and Fig. 4(d). The raw hologram contains spectral components corresponding to zero-order noise and the twin image in the Fourier domain, which are the unwanted spectral components that act as the noise making the beating profile of the CM unobtainable, so the Int $_{var}$ -Raw-Holo is observed to be very noisy, as shown in Fig. 4(c). In contrast, the filtered hologram contains only spectral component corresponding to the real image, so the Int $_{var}$ -Filtered-Holo is better observed.

Meanwhile, when the optical flow method is used, it is possible to measure the lateral motion between successive raw holograms even in the presence of noise, as shown in Speed-OptF-Raw-Holo in Fig. 4(e). Figures 4(e) and 4(f) show the contractile beating profiles of CMs obtained using the proposed method, i.e., applying optical flow to raw and filtered holograms, respectively. These results confirm that by using the proposed method, it is possible to obtain sufficiently contractile beating profiles of CMs that are comparable to those obtained using the existing method.

3.2. Effects of isoprenaline drug-treatment

We compared contraction motion-speed before and after treatment with a medication to describe pharmacological effects on the CM's contractile motion-speed. The other characteristics, on the other hand, were assessed to precisely determine the drug's effects. The effects of the compounds were obvious in critical-parameter measurement results. To begin, we conducted an experiment

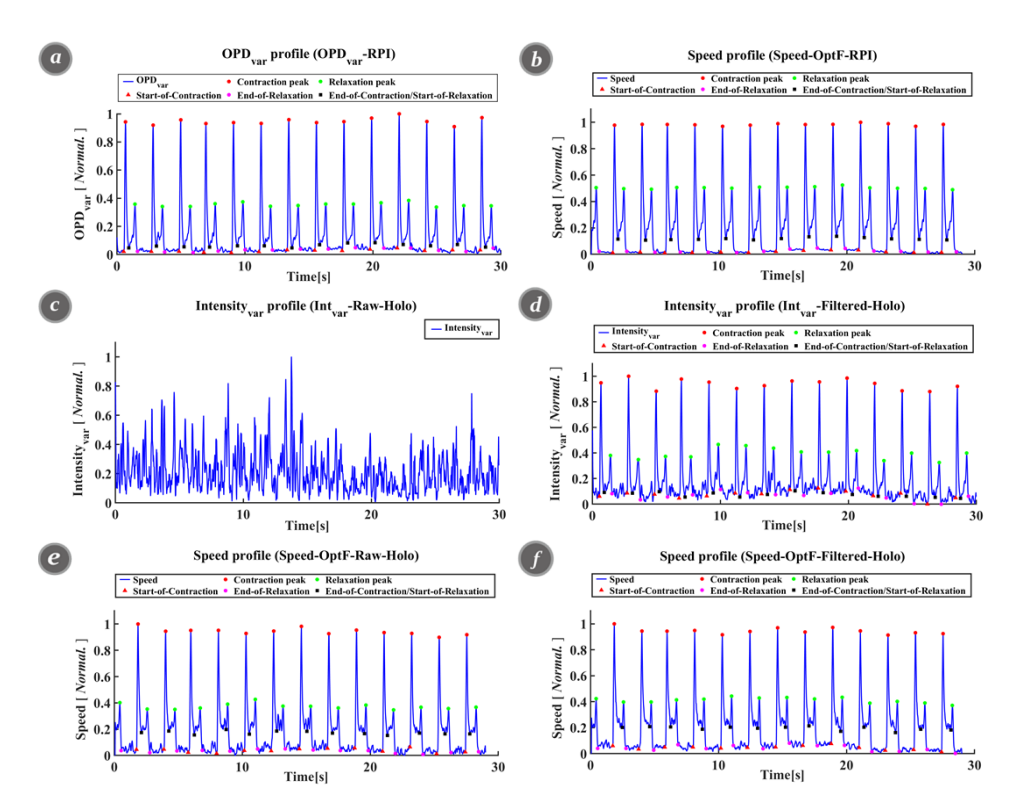


Fig. 4. Comparison of contractile dynamics (i.e., motion-speed dynamics) of CMs: (a) using variance of OPD difference between successive RPIs, i.e., OPD-based beating signal, (b) applying the optical flow method to the RPIs, (c) using variance of intensity difference between successive raw holograms, (d) using variance of intensity difference between successive filtered holograms, (e) applying the optical flow method to raw holograms, (f) applying the optical flow method to filtered holograms. The contractile motion-speed profiles of the CM are normalized. RPI represents the reconstructed phase image, OptF represents the optical flow, OPD_{var} represents the variance of OPD difference between successive RPIs, i.e., Eq. (1), and Int_{var} represents the variance of intensity difference between successive raw or filtered holograms.

to determine the effects of isoprenaline. The isoprenaline molecule is a β -1 and β -2 adrenergic receptor agonist that works by stimulating the G-alpha second messenger pathway [45]. In response to isoprenaline, the related quantification data of the contractile motion waveform of the whole-slide images (i.e., raw holograms, filtered holograms, or RPIs) of CMs in control versus Isoprenaline drug-treated circumstances is shown in Fig. 5. Figure 5(c) and Fig. 5(d) show that as Isoprenaline concentration increases, resting periods and, in turn, beating periods decrease compared to the control condition. Contraction periods and relaxation periods become smaller than in control conditions with increasing isoprenaline concentration, but do not decrease as drastically as do resting periods, as shown in Fig. 5(a) and Fig. 5(b). Therefore, Isoprenaline, a non-selective β -adrenoceptor agonist, primarily reduces the resting period, which decreases the overall duration of each beat, thereby increasing the beating frequency [46]. Table 1 shows beating rates (or beating frequency) in cycles per minute in the presence of different Isoprenaline concentrations versus control conditions.

As shown in the cases of OPD_{var}-RPI (black line) and Speed-OptF-RPI (blue line) in Fig. 5, it can be seen that the temporal parameters such as contraction periods, relaxation periods, resting

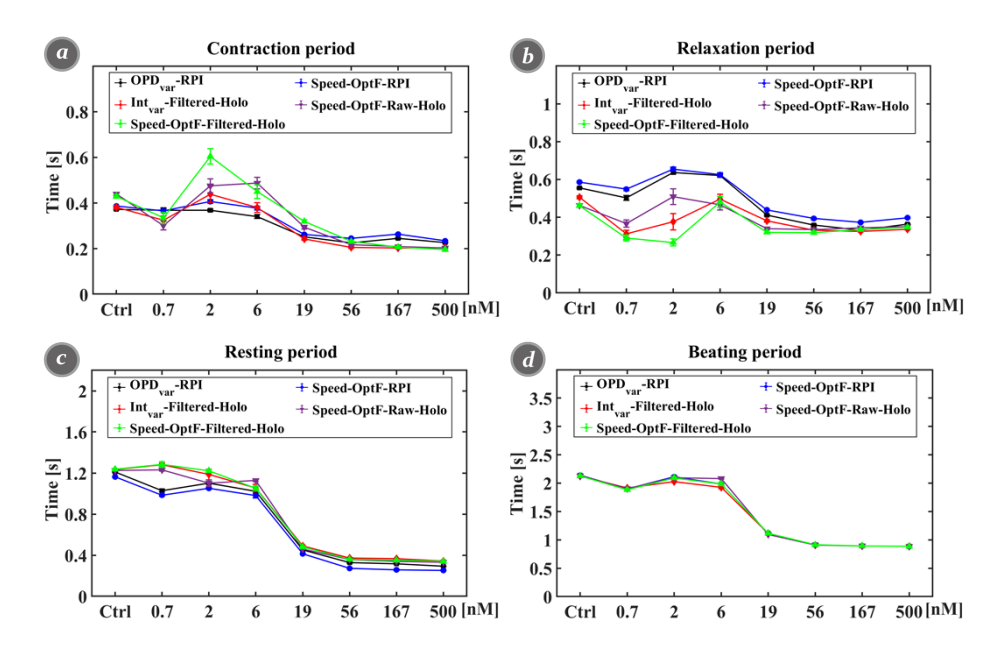


Fig. 5. The temporal quantification results of the contractile motion waveforms over whole-slide images of CMs in the presence of different Isporenaline concentrations versus control conditions. (a) Contraction periods, (b) relaxation periods, (c) resting periods, and (d) beating periods. RPI represents the reconstructed phase image, OPD_{var} represents the variance of OPD difference between successive RPIs, i.e., Eq. (1), OptF represents the optical flow, and Int_{var} represents the variance of intensity difference between successive raw or filtered holograms. The bar charts show the variations of the critical parameter expressed in terms of mean and standard error in control versus drug-treated conditions in presence of different drug concentrations. Error bars represent standard errors.

Table 1. Beating rates in the presence of different Isoprenaline concentrations versus control conditions (cycles/min).

	Control	0.7 nM	2 nM	6 nM	19 nM	56 nM	167 nM	500 nM
OPD _{var} – RPI ^a	28.086	31.564	28.472	30.243	53.897	65.849	67.154	67.848
Speed-OptF-RPI	28.098	31.571	28.432	30.248	53.856	65.822	67.076	67.817
Int _{var} -Filtered-holograms	28.267	31.297	29.605	31.123	53.831	65.942	67.164	67.785
Speed-OptF-Raw-holograms	28.198	31.519	28.604	28.822	54.769	65.886	67.126	67.837
Speed-OptF-Filtered-holograms	28.201	31.839	28.670	30.209	53.812	65.838	67.153	67.805

^aRPI : Reconstructed phase image.

periods, and beating periods, which are obtained by the existing method, i.e., calculating the variance of OPD difference between successive RPIs (OPD_{var}-RPI in Fig. 5) or applying the optical flow method to the RPIs (Speed-OptF-RPI in Fig. 5), are almost close to each other. These results confirm that the contraction-relaxation beating profiles in the lateral direction (*x-y* direction in Fig. 1(a)) and the optical axis direction (*z* direction in Fig. 1(a)) of CMs can be equally obtained by applying the optical flow method to the RPIs and calculating the variance of OPD difference between successive RPIs, i.e., Eq. (1). Meanwhile, as shown in Fig. 5(a) and Fig. 5(b), the contraction and relaxation periods obtained by the proposed methods, i.e., by applying the optical flow method to raw and filtered holograms (Speed-OptF-Raw-Holo and Speed-OptF-Filtered-Holo), and by calculating the variance of the intensity difference between

Table 2. Beating rates in the presence of different E-4031 concentrations versus control conditions (cycles/min).

	Control	3 uM	10 uM	30 uM	100 uM
OPD _{var} - RPI ^a	26.563	25.441	21.107	12.759	10.870
Speed-OptF-RPI	26.537	25.503	21.141	12.759	10.903
Int _{var} -Filtered holograms	26.553	25.399	21.204	12.766	10.928
Speed-OptF-Raw-holograms	26.528	25.390	21.136	12.781	10.889
Speed-OptF-Filtered-holograms	26.539	25.444	21.124	12.701	10.982

^aRPI : Reconstructed phase image.

successive filtered holograms (Int_{var}-Filtered-Holo in Fig. 5) are quite different from those obtained by the existing methods, i.e., OPD_{var}-RPI and Speed-OptF-RPI. However, as shown in Fig. 5(c), the resting period obtained by the proposed method is almost close to that obtained by the exiting methods at high Isoprenaline drug concentrations (above 6 nM). Especially, as shown in Fig. 5(d), the beating periods obtained by the five methods are perfectly consistent with each other except for two Isoprenaline drug concentrations. In addition, for the resting periods and beating periods, all temporal parameters obtained by calculating the variance of the intensity difference between successive filtered holograms, i.e., Int_{var}-Filtered-Holo (red line) in Fig. 5, are closer to those obtained by applying the optical flow method to filtered holograms, i.e., Speed-OptF-Filtered-Holo (green line) in Fig. 5. Finally, as shown in Table 1, the beating rates obtained using the four methods are very consistent with each other, which means that it is possible to estimate beating rates (or beating frequency) from raw or filtered holograms without the need for reconstruction and phase unwrapping.

3.3. Effects of E-4031 drug-treatment

We looked at how E-4031 affected the motion waveform of CMs. The inactivating inward rectifying potassium current IKR is blocked by E-4031, which is a strong and specific blocker (HERG channel). The treatment of CMs with E-4031 was found to considerably lower the heart rate, enhance myocardial Ca²⁺ uptake, and reduce intracellular K⁺ loss in cardiac cells [46–48]. In response to E-4031, the contractile motion in the whole-slide images of CMs in control and E-4031 drug-treated circumstances is shown in Fig. 6. For control and E-4031 drug-treated circumstances, the contraction and relaxation periods vary little depending on concentration, although there are subtle variations (Fig. 6(a) and Fig. 6(b)). However, as shown in Fig. 6(c) and Fig. 6(d), the associated beating and resting periods are both greatly extended, resulting in a decrease in the beating rates (or beating frequency). So, the degree of change in beating rates varied significantly between different levels of drug concentration. Different concentrations of E-4031 dramatically change resting periods, such that increasing E-4031 concentration results in an increase in beating period. Table 2 shows the beating rates in cycles per minute in the presence of different E-4031 concentrations versus control conditions.

Similar to the cases of Isoprenaline, as shown in the cases of OPD_{var} -RPI (black line) and Speed-OptF-RPI (blue line) in Fig. 6, it can be seen that the temporal parameters obtained by existing methods, i.e., calculating the variance of OPD difference between successive RPIs (OPD_{var}-RPI) or applying the optical flow method to the RPIs (Speed-OptF-RPI), are almost the same as each other. On the other hand, as shown in Fig. 6(a) and Fig. 6(b), contraction and relaxation periods obtained by the proposed methods, i.e., applying the optical flow method to raw and filtered holograms (Speed-OptF-Raw-Holo and Speed-OptF-Filtered-Holo), are quite different from those obtained with the existing methods. Nevertheless, as shown in Fig. 6(c) and Fig. 6(d), the resting period obtained by the proposed methods is almost close to that obtained by the existing methods, and especially the beating periods obtained by the five methods are

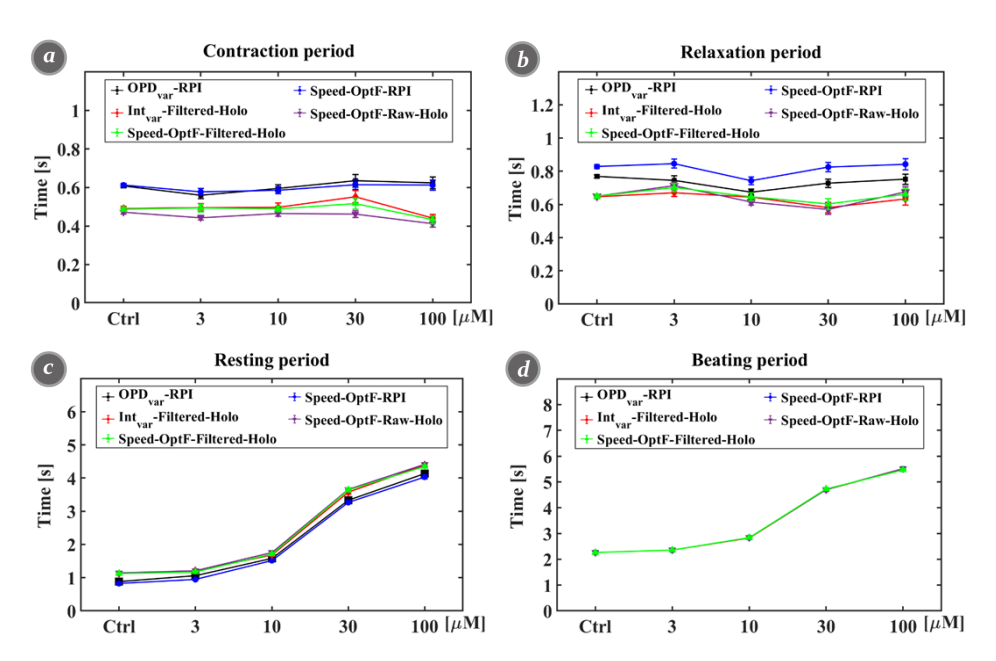


Fig. 6. The temporal quantification results of the contractile motion waveforms over whole-slide images of CMs in the presence of different E-4031concentrations versus control conditions. (a) Contraction periods, (b) relaxation periods, (c) resting periods, and (d) beating periods. RPI represents the reconstructed phase image, OPD_{var} represents the variance of OPD difference between successive RPIs, i.e., Eq. (1), OptF represents the optical flow, and Int_{var} represents the variance of intensity difference between successive raw or filtered holograms. The bar charts show the variations of the critical parameter expressed in terms of mean and standard error in control versus drug-treated conditions in presence of different drug concentrations. Error bars represent standard errors.

perfectly consistent with each other for all Isoprenaline drug concentrations. As in the cases of Isopreline, all temporal parameters obtained by calculating the variance of the intensity difference between successive filtered holograms, i.e., Int_{var}-Filtered-Holo (red line) in Fig. 6, are closer to those obtained by applying the optical flow method to filtered holograms, i.e., Speed-OptF-Filtered-Holo (green line) in Fig. 6. As shown in Table 2, the beating rates (or beating frequency) can be estimated from the raw or filtered hologram without the need for reconstruction and phase unwrapping, as in the cases of Isopreline.

4. Discussion and future work

The 3D reconstruction of hologram of cells such as red blood cells or CMs is necessary to accurately and specifically measure or track the dynamic behavior of the cells or to explore cardiomyocyte functions such as morphological changes. Moreover, one advantage of digital holography is that DHM can perform automatic digital focusing. But the proposed method cannot perform automatic digital focusing since it no longer performs hologram reconstruction.

Despite not being able to take advantage of the DHM's ability to autofocus, we chose DHM as an imaging method simply to compare the contraction dynamics of CMs when directly applying the optical flow method to cells with that when using phase-reconstructed images, where they can be performed together. Holograms can be acquired efficiently using compact DHM, such as lateral shearing digital holographic microscope, presented for cell analysis [3]. If the off-axis DHM is used for the acquisition of raw holograms, the spectrum corresponding to the real image can be easily filtered from the raw hologram to obtain a filtered hologram. Additionally, when

recording temporally sequential holograms of cardiomyocytes, once the DHM is manually set up to record in focus to obtain a hologram with high image quality in the first frame, holograms in subsequent frames can be captured without any additional adjustments.

Meanwhile, since the raw hologram contains spectrum corresponding to the real image, the zero-noise spectrum and spectrum corresponding to the twin image, and the higher-order spectra, the temporal contractile dynamics based on the variance of the intensity variance are superimposed, making it impossible to monitor the contractile dynamics of the CMs. However, when applying the optical flow method, which measures the lateral movement of a pixel with a specific intensity, to the raw hologram, the temporal contractile dynamics of the CMs can be monitored. Generally, the spacing between the fringes in the interference pattern in the interferogram (i.e., recorded digital hologram) reflects the phase information of the sample, i.e., the thickness of sample. Then, when the CMs beat, these fringes will be shifted, especially in the boundary region of the CMs. This means that it may be possible to monitor the contractile dynamics of the CMs using the optical flow method. Additionally, a thorough and detailed study of the noise sensitivity, the image quality dependency, and hardware constraints caused when applying optical flow methods to raw or filtered holograms is a challenge that requires further research in the future.

Another limitation of the proposed method is the difficulty in determining the end-of-contraction/start-of-relaxation points in the contraction-relaxation motion speed profile. This can reduce the accuracy of measuring contraction and relaxation periods. However, despite this difficulty, the beating period was measured identically when each of the five different methods was used. Finally, the proposed scheme can obtain the same beating rate of CMs as obtained from reconstructed phase images by directly applying the optical flow method to raw or filtered holograms to track the contraction-relaxation motion-speed profile of CMs without the need for numerical phase image reconstruction.

Despite several difficulties, the proposed scheme provides a streamlined method to track the contraction-relaxation motion-speed of cardiomyocyte beating by applying optical flow methods to raw or filtered holograms. The beating rates (or the beating periods) were quite consistent with those obtained when applying the optical flow method to the reconstructed phase images. This shows the potential to track the dynamic contraction-relaxation motion-speed of CMs in response to drug-treatment by directly applying optical flow method to raw or filtered holograms without phase reconstruction and phase unwrapping. This also suggests that it opens the possibility of tracking the dynamic contraction-relaxation motion-speed of CMs in response to drug-treatment from raw or filtered holograms obtained using other compact DHMs, if not larger off-axis DHMs.

Next, phase contrast microscopy makes it difficult to extract quantitative information from a specimen because the observed image appears mixed with background intensity. The main limitation of differential interference contrast (DIC) is that it requires a transparent sample with a refractive index fairly similar to that of the surrounding environment (a refractive index difference of around 0.05). DIC is not suitable in biology for thick samples such as tissue slices and highly pigmented cells. When using non-quantitative phase microscopy techniques such as DIC for CM dynamics, automating focus becomes difficult due to the need to manually find the (focused) image plane. Furthermore, DIC images are largely free of the halo and shade-off effects artifacts that degrade the image quality in phase contrast optical systems. However, although configuration modifications to the objective phase plate design can suppress halos to a limited extent, they cannot be eliminated. In DIC, areas of light and shadow may be enhanced, distorting the image appearance.

Nevertheless, several commercial technologies and systems are available to track the beating dynamics of CMs. Tadano et al. analyzed the dynamics of cardiomyocyte beating using the flow method of the SI8000 cell motion imaging system (Sony, Tokyo, Japan), which records phase contrast images using a phase-contrast microscope [49]. They reported that the beating rates of

CMs decreased when CMs were drug-treated with E-4031 at increased concentrations. They also reported that when drug-treated with Isoprenaline at increased concentrations, the beating rates of CMs increased, but when drug-treated with Isoprenaline at high concentrations (30-1,000 nM), the beating rates almost plateaued [49]. These results agree with those of our proposed approach. As another case, FDSS/µCell (Hamamatsu Ltd., Hamamatsu, Japan) can be used to analyze the dynamics of cardiomyocyte beating [50]. This commercial platform is a high-speed acquisition imaging platform that allows simultaneous high-throughput readout of fluorescence signals (intensity) under controlled physiological temperature. Despite these advantages, the fluorescence-based system for analyzing CM beating has drawbacks such as damage to CMs caused by fluorescent substances and short duration of emission of fluorescent substances. On the other hand, the proposed method is non-invasive and allows single-shot holographic recording (i.e., recording interferograms containing phase information), making it suitable for live imaging. It is a label-free (i.e., unstained) method for acquiring high-speed quantitative phase images of architecture and contractile dynamics of CMs.

Another approach to monitor the contractile dynamics of CMs is QPI-based cell analysis, which utilizes digital holography technique that is non-invasive and allows single-shot recording. However, the approach requires the reconstruction stage, which can be difficult and time-consuming because it necessitates numerical reconstruction and then phase unwrapping. Furthermore, the contractile dynamics of CMs have never been analyzed based on off-axis holograms. By merging the Farnebäck optical flow method and digital holograms for cardiotoxicity screening, we were able to track the contractile motion of CMs using raw or filtered holograms without the need for reconstruction. The main advantage of this proposal relies on the fact that the numerical reconstruction procedure traditionally used in DHM can be completely avoided.

The proposed system includes two parts. First, we calculated the contractile motion-speed of beating cells using the Farnebäck optical flow method. Second, we developed a computational algorithm that provided further complementary information about critical parameters regarding a CM's beating activity profile. In this study, the contractile characteristics of drug-treated CMs can be evaluated by measuring changes in beating rates (or beating frequency), as well as other comparable baseline parameters, from raw or filtered holograms, allowing measuring hiPSC kinetic responses to drugs that cannot be identified using conventional methods. The effects of two compounds (Isoprenaline and E-4031) were studied at various concentrations. The results of our experiments with E-4031 and Isoprenaline were in good agreement with those of a prior study [19,35,51]. Isoprenaline speeds up the contractile motion, but E-4031 causes the contractile motion to slow down. Both medicines altered the resting period, in turn, beating period, resulting in a change in the frequency of the heartbeat. The purpose of these investigations was to assess other crucial metrics related to the beating activity profile generated utilizing contractile motion-speed measurement in addition to monitoring the kinetics from raw or filtered holograms. Furthermore, this result also suggests that it opens the possibility of tracking contraction-relaxation motion dynamics of CMs in response to drug-treatment from raw or filtered holograms obtained using compact DHMs [52,53], even if not larger off-axis DHMs.

In the proposed method, it takes an average of 0.234 seconds to track the contraction-relaxation motion-speed profile of CMs from one frame of video of holograms using the Farnebäck optical flow method. This is long compared to hologram video's frame rate of 0.1 seconds per frame, which makes it difficult to track the contraction-relaxation motion-speed profile of CMs in real-time. Nevertheless, the proposed method has the advantage that it does not require numerical reconstruction and phase unwrapping, whereas conventional approaches related to holograms typically require them. As a result, the proposed method enables rapid contractile dynamic analysis of CMs compared to existing approaches, which require reconstruction. Several studies have reported on the time required to perform numerical reconstruction [54–56]. Jaferzadeh et al. reported that the phase reconstruction rate was 15 frames per second, or 0.667 seconds per

frame [54]. Park et al. reported that the reconstruction takes about 1.93 seconds per hologram, including numerical propagation, autofocus, phase unwrapping, and reference wave calculation [55]. Rivenson et al. reported that it takes approximately 7.85 seconds for a field of view of 1mm^2 of the image when using the method proposed by the authors [56], which corresponds to approximately 0.707 seconds for the holograms $(0.3 \times 0.3 \text{ mm}^2)$ used in the proposed method. For one hologram, the reconstruction process itself in the existing methods takes approximately three times more than the process of tracking the contraction-relaxation motion-speed profile using optical flow in the proposed method. In other words, that much time can be saved.

Lastly, various AI-based approaches are proposed, such as cell identification or cell classification of red blood cells or cancer cells, cell disease identification [57,58], or pixel classification technique at the single-cell level [43]. To our knowledge, there has been no AI-based study on the contractile dynamics of CMs and the cardiotoxicity assessment of drugs, which are measured by directly applying the optical flow method to raw or filtered holograms. An AI model learns the patterns in the given data, which means that not only a large amount of data is required, but also a wide variety of data types are essential to avoid biased and unstable outcomes. Therefore, a large and diverse dataset is crucial to developing models with reliable performance. However, since culturing CMs is time-consuming and costly, gathering a sufficiently extensive and diverse set of data, whole-slide images of CMs, for training models to analyze the contractile dynamics of CMs becomes incredibly challenging. Then, such AI-based studies are a difficult challenge that we will have to perform in the future.

5. Conclusion

In this article, we present an automated fast label-free method for contractile dynamic analysis of CMs by applying the Farnebäck optical flow method directly to raw or filtered holograms for cardiotoxicity screening. Generally, temporal parameters related to CMs can be measured more accurately by applying the optical flow method to the RPIs or calculating the variance of OPD difference between successive RPIs. However, the proposed method enables dynamic analysis of CMs, particularly resting periods and beating periods (in turn, beating rates), by applying the optical flow method directly to raw or filtered holograms without the need for complicated and time-consuming numerical reconstructions and phase unwrapping.

In the proposed method, contractile characteristics of drug-treated CMs can be evaluated by measuring changes in beating rates (or beating frequency) and other comparable baseline parameters that indicate hiPSC kinetic responses to drugs from raw or filtered holograms. Experimental results on contractile dynamics of CMs for two compounds (Isoprenaline and E-4031) with various concentrations confirm that they change the hearting rates (or beating frequency) of CMs by changing resting periods of CMs. In addition, the results confirm that Isoprenaline speeds up the contractile motion of CMs, but E-4031 causes the contractile motion to slow down.

Funding. National Research Foundation of Korea (RS-2023-00253613).

Disclosures. The authors declare that they have no known competing financial interests or personal relationships that could have appeared to influence the work reported in this paper.

Data availability. Data underlying the results presented in this paper are not publicly available at this time but may be obtained from the authors upon reasonable request.

References

- I. Madan, G. M. Vanacore, E. Pomarico, et al., "Holographic imaging of electromagnetic fields via electron-light quantum interference," Sci. Adv. 5(5), eaav8358 (2019).
- H. Ren, W. Shao, Y. Li, et al., "Three-dimensional vectorial holography based on machine learning inverse design," Sci. Adv. 6(16), eaaz4261 (2020).
- 3. B. Javid, A. Markman, S. Rawat, *et al.*, "Sickle cell disease diagnosis based on spatio-temporal cell dynamics analysis using 3D printed shearing digital holographic microscopy," Opt. Express **26**(10), 13614–13627 (2018).

- T. O'Connor, A. Anand, B. Andemariam, et al., "Deep learning-based cell identification and disease diagnosis
 using spatio-temporal cellular dynamics in compact digital holographic microscopy," Biomed. Opt. Express 11(8),
 4491–4508 (2020).
- 5. T. O'Connor, S. Santaniello, and B. Javidi, "COVID-19 detection from red blood cells using highly comparative time-series analysis (HCTSA) in digital holographic microscopy," Opt. Express 30(2), 1723–1736 (2022).
- B. Javid, I. Moon, S. Yeom, et al., "Three-dimensional imaging and recognition of microorganism using single-exposure on-line (SEOL) digital holography," Opt. Express 13(12), 4492–4506 (2005).
- B. Javid, S. Yeom, I. Moon, et al., "Real-time automated 3D sensing, detection, and recognition of dynamic biological micro-organic events," Opt. Express 14(9), 3806–3829 (2006).
- M. Liebel, J. O. Arroyo, V. S. Beltrán, et al., "3D tracking of extracellular vesicles by holographic fluorescence imaging," Sci. Adv. 6(45), eabc2508 (2020).
- S. N. Chen, C. K. Lam, Y.-W. Wan, et al., "Activation of PDGFRA signaling contributes to filamin C-related arrhythmogenic cardiomyopathy," Sci. Adv. 8(8), eabk0052 (2022).
- I. Moon, E. Ahmadzadeh, K. Jaferzadeh, et al., "Automated quantification study of human cardiomyocyte synchronization using holographic imaging," Biomed. Opt. Express 10(2), 610–621 (2019).
- B. Rappaz, E. Cano, T. Colomb, et al., "Noninvasive characterization of the fission yeast cell cycle by monitoring dry mass with digital holographic microscopy," J. Biomed. Opt. 14(3), 034049 (2009).
- S. J. Kim, C. Wang, B. Zhao, et al., "Deep transfer learning-based hologram classification for molecular diagnostics," Sci. Rep. 8(1), 17003 (2018).
- 13. T. Go, S. Lee, D. You, *et al.*, "Deep learning-based hologram generation using a white light source," Sci. Rep. **10**(1), 8977 (2020).
- D. Schocken, J. Stohlman, J. Vicente, et al., "Comparative analysis of media effects on human induced pluripotent stem cell-derived cardiomyocytes in Proarrhythmia risk assessment," J. Pharmacol. Toxicol. Methods 90, 39–47 (2018).
- 15. J. K. Gibson, Y. Yue, J. Bronson, *et al.*, "Human stem cell-derived cardiomyocytes detect drug-mediated changes in action potentials and ion currents," J. Pharmacol. Toxicol. Methods **70**(3), 255–267 (2014).
- N. T. Shaked, L. L. Satterwhite, N. Bursac, et al., "Whole-cell-analysis of live cardiomyocytes using wide-field interferometric phase microscopy," Biomed. Opt. Express 1(2), 706–719 (2010).
- 17. I. Moon, M. Daneshpanah, B. Javidi, *et al.*, "Automated three-dimensional identification and tracking of micro/nanobiological organisms by computational holographic microscopy," Proc. IEEE **97**(6), 990–1010 (2009).
- J. Kühn, E. Shaffer, J. Mena, et al., "Label-free cytotoxicity screening assay by digital holographic microscopy," Assay Drug Dev. Technol. 11(2), 101–107 (2013).
- K. Jaferzadeh, B. Rappaz, F. Kuttler, et al., "Marker-free automatic quantification of drug-treated cardiomyocytes with digital holographic imaging," ACS Photonics 7(1), 105–113 (2020).
- 20. T. Colomb, F. Charrière, J. Kühn, et al., "Advantages of digital holographic microscopy for real-time full field absolute phase imaging," in *Proceedings of the Three-Dimensional and Multidimensional Microscopy: Image Acquisition and Processing XV*, (San Jose, CA, USA, 2008), pp. 686109.
- E. Cuche, P. Marquet, and C. Depeursinge, "Spatial filtering for zero-order and twin-image elimination in digital off-axis holography," Appl. Opt. 39(23), 4070–4075 (2000).
- E. Cuche, P. Marquet, and C. Depeursinge, "Simultaneous amplitude-contrast and quantitative phase-contrast microscopy by numerical reconstruction of Fresnel off-axis holograms," Appl. Opt. 38(34), 6994

 –7001 (1999).
- U. Schnars and W. P. O. Jüptner, "Digital recording and numerical reconstruction of holograms," Meas. Sci. Technol. 13(9), R85–R101 (2002).
- C. Trujillo and J. Garcia-Sucerquia, "Automatic detection and counting of phase objects in raw holograms of digital holographic microscopy via deep learning," Opt. Lasers Eng. 120, 13–20 (2019).
- M. K. Kim, L. Yu, and C. J. Mann, "Interference techniques in digital holography," J. Opt. A: Pure Appl. Opt. 8(7), S518–S523 (2006).
- M. Arevalillo-Herráez, D. R. Burton, M. J. Lalor, et al., "Fast two-dimensional phase-unwrapping algorithm based on sorting by reliability following a noncontinuous path," Appl. Opt. 41(35), 7437 (2002).
- D. Ossola, M. Y. Amarouch, P. Behr, et al., "Force-controlled patch clamp of beating cardiac cells," Nano Lett. 15(3), 1743–1750 (2015).
- 28. A. Brüggemann, C. Haarmann, M. Rapedius, et al., "Characterization of iPS derived cardiomyocytes in voltage clamp and current clamp by automated patch clamp," Biophys. J. 112(3), 236a (2017).
- O. Sirenko, C. Crittenden, N. Callamaras, et al., "Multiparameter in vitro assessment of compound effects on cardiomyocyte physiology using iPSC cells," J. Biomol. Screen 18(1), 39–53 (2013).
- G. T. Dempsey, K. W. Chaudhary, N. Atwater, et al., "Cardiotoxicity screening with simultaneous optogenetic pacing, voltage imaging and calcium imaging," J. Pharmacol. Toxicol. Methods 81, 240–250 (2016).
- 31. E. Grespan, S. Martewicz, E. Serena, et al., "Analysis of calcium transients and uniaxial contraction force in single human embryonic stem cell-derived cardiomyocytes on microstructured elastic substrate with spatially controlled surface chemistries," Langmuir 32(46), 12190–12201 (2016).
- 32. C. Bazan, D. T. Barba, P. Blomgren, *et al.*, "Image processing techniques for assessing contractility in isolated neonatal cardiac myocytes," Int. J. Biomed. Imaging **2011**, 1–9 (2011).

- 33. N. Huebsch, P. Loskill, M. A. Mandegar, *et al.*, "Automated video-based analysis of contractility and calcium flux in human-induced pluripotent stem cell-derived cardiomyocytes cultured over different spatial scales," Tissue Eng. Part C Methods **21**(5), 467–479 (2015).
- 34. A. Czirok, D. G. Isai, E. Kosa, *et al.*, "Optical-flow based non-invasive analysis of cardiomyocyte contractility," Sci. Rep. **7**(1), 10404 (2017).
- 35. P. Hoang, N. Huebsch, S. H. Bang, *et al.*, "Quantitatively characterizing drug-induced arrhythmic contractile motions of human stem cell-derived cardiomyocytes," Biotechnol. Bioeng. **115**(8), 1958–1970 (2018).
- 36. G. Farnebäck, "Two-frame motion estimation based on polynomial expansion," in J. Bigun and T. Gustavsson, eds., Image Analysis. SCIA 2003. LNCS, vol 2749, (Springer, Berlin, Heidelberg, 2003), pp. 363–370.
- 37. E. Ahamadzadeh, K. Jaferzadeh, S. Park, et al., "Automated analysis of human cardiomyocytes dynamics with holographic image-based tracking for cardiotoxicity screening," Biosens. Bioelectron. 195, 113570 (2022).
- 38. L. Yu and M. K. Kim, "Wavelength-scanning digital interference holography for tomographic 3D imaging using the angular spectrum method," Opt. Lett. 30(16), 2092–2094 (2005).
- B. Rappaz, I. Moon, F. Yi, et al., "Automated multi-parameter measurement of cardiomyocytes dynamics with digital holographic microscopy," Opt. Express 23(10), 13333–13347 (2015).
- K. Jaferzadeh, B. Rappaz, Y. Kim, et al., "Automated dual-mode cell monitoring to simultaneously explore calcium dynamics and contraction-relaxation kinetics within drug-treated stem cell-derived cardiomyocytes," ACS Sens. 8(7), 2533–2542 (2023).
- 41. J. L. Barron, D. J. Fleet, and S. S. Beauchemin, "Performance of optical flow techniques," Int. J. Comput. Vis. 12(1), 43–77 (1994).
- 42. B. D. Lucas and T. Kanade, "An iterative image registration technique with an application to stereo vision," in *Proceedings of the 7th International Joint Conference on Artificial Intelligence* vol. 2, (Morgan Kaufmann Publishers Inc., San Francisco, CA, USA, 1981), pp. 674–679.
- 43. E. Ahmadzadeh, K. Jaferzadeh, S. Shin, *et al.*, "Automated single cardiomyocyte characterization by nucleus extraction from dynamic holographic images using a fully convolutional neural network," Biomed. Opt. Express 11(3), 1501–1516 (2020).
- S. J. Roy and P. S. Mainzen Prince, "Protective effects of sinapic acid on cardiac hypertrophy, dyslipidaemia and altered electrocardiogram in isoproterenol-induced myocardial infarcted rats," Eur. J. Pharmacol. 699(1-3), 213–218 (2013).
- T. Hayakawa, T. Kunihiro, T. Ando, et al., "Image-based evaluation of contraction-relaxation kinetics of human-induced pluripotent stem cell-derived cardiomyocytes: Correlation and complementarity with extracellular electrophysiology," J. Mol. Cell. Cardiol. 77, 178–191 (2014).
- 46. Q. Zhao, X. Wang, S. Wang, et al., "Cardiotoxicity evaluation using human embryonic stem cells and induced pluripotent stem cell-derived cardiomyocytes," Stem Cell Res. Ther. 8(1), 54 (2017).
- 47. J. Q. He, Y. Ma, Y. Lee, *et al.*, "Human embryonic stem cells develop into multiple types of cardiac myocytes: Action potential characterization," Circ. Res. **93**(1), 32–39 (2003).
- 48. C. Luo, K. Wang, and H. Zhang, "Modelling the effects of quinidine, disopyramide, and E-4031 on short QT syndrome variant 3 in the human ventricles," Physiol. Meas. **38**(10), 1859–1873 (2017).
- K. Tadano, S. Miyagawa, M. Takeda, et al., "Cardiotoxicity assessment using 3D vascularized cardiac tissue consisting of human iPSC-derived cardiomyocytes and fibroblasts," Mol. Ther. -Methods Clin. Dev. 22, 338–349 (2021).
- H. Zeng, M. I. Roman, E. Lis, et al., "Use of FDSS/μCell imaging platform for preclinical cardiac electrophysiology safety screening of compounds in human induced pluripotent stem cell-derived cardiomyocytes," J. Pharmacol. Toxicol. Methods 81, 217–222 (2016).
- I. Moon, K. Jaferzadeh, E. Ahmadzadeh, et al., "Automated quantitative analysis of multiple cardiomyocytes at the single-cell level with three-dimensional holographic imaging informatics," J. Biophotonics 11(12), e201800116 (2018).
- 52. A. Anand, V. K. Chhaniwal, and B. Javid, "Real-time digital holographic microscopy for phase contrast 3D imaging of dynamic phenomena," J. Disp. Technol. 6(10), 500–505 (2010).
- 53. A. Anand, V. K. Chhaniwal, and B. Javidi, "Imaging embryonic stem cell dynamics using quantitative 3-D digital holographic microscopy," IEEE Photonics J. 3(3), 546–554 (2011).
- 54. K. Jaferzadeh, S. Son, A. Rehman, *et al.*, "Automated stain-free holographic image-based phenotypic classification of elliptical cancer cells," Adv. Photonics Res. **4**(1), 2200043 (2023).
- S. Park, Y. Kim, and I. Moon, "Fast automated quantitative phase reconstruction in digital holography with unsupervised deep learning," Opt. Lasers Eng. 167, 107624 (2023).
- Y. Rivenson, Y. Zhang, H. Günaydın, et al., "Phase recovery and holographic image reconstruction using deep learning in neural networks," Light: Sci. Appl. 7(2), 17141 (2017).
- 57. G. Aschenbrenner, S. Goswami, K. Usmani, et al., "Review: advances in lensless random phase encoded imaging for automated cell identification," Opt. Eng. 63(11), 111814 (2024).
- 58. P. M. Douglass, T. O'Connor, and B. Javidi, "Automated sickle cell disease identification in human red blood cells using a lensless single random phase encoding biosensor and convolutional neural networks," Opt. Express 30(20), 35965–35977 (2022).